Applied Water Science (2021) 11:51
https://doi.org/10.1007/s13201-021-01380-x

ORIGINAL ARTICLE

Preparation of flexible electrospun AOPAN/PVDF membranes for removing Pb^{2+} from water

Yang Chen[1] · Lanying Jiang[1,2,3]

Received: 13 November 2020 / Accepted: 4 February 2021 / Published online: 22 February 2021

Abstract

Electrospun AOPAN/PVDF composite nanofiber membranes for metal ions treatment have been prepared by coaxial electrospinning. AOPAN shell layer was modified chemically for adsorbing metal ions by chelation, whereas the chemically stable PVDF inner core was for maintaining mechanical stability. Polymer concentration and applied voltage had obvious influence on the characteristics of the fibers' structure, morphology and strength. The amidoxime reaction was sensitive to the pH value of solution, and it was found that the alkaline condition hindered the reaction. The characterization by SEM, FTIR and XRD showed that the AOPAN/PVDF membrane retained the core–shell structure integrity after chemical modification. In the static and dynamic adsorption experiments, the mechanical strength of the AOPAN/PVDF membrane did not change obviously within 5 cycles of adsorption and regeneration. In addition, the AOPAN/PVDF membranes showed a certain level of efficiency in removal of Pb^{2+} in aqueous solution; the adsorption capacities of the membranes in the 5th run were higher than 45% of the adsorption of the corresponding fresh membranes. The work provides a potential approach for preparing membranes having good feasibility for practical application in adsorption separation of metal ions.

Keywords Coaxial electrospinning · Membrane durability · Amidoxime · Pb^{2+} removal

Introduction

Heavy metals are among the pollutants that have toxicological effects on humans (Järup 2003). Some heavy metals are associated with destroying cellular structure and thus life-threatening. Therefore, progressively stricter limit for the levels of environmental heavy metals have been enforced (Jobby et al. 2018; Wu et al. 2019; Wang et al. 2017). Water is for everybody indispensably, and water pollution has always been the focus in environmental protection. A series of exogenous and endogenous control have been investigated and/or applied for tackling heavy metals in aquatic system (Fu and Wang 2011). They are mainly relying on chemical precipitation, coagulation and flocculation, membrane filtration, ion exchange, electrochemical methods and adsorption (). All these technologies are featured with flexible design and easy operation. The strength of adsorption lies in the combination of its selectivity toward minor components and high removal efficiency. Therefore, it is of particular interest for treating heavy metals at low concentrations and generally adopted as a polishing step for wastewater processing (Xiaolei and P.J. J. A. 2013).

For practical application, a good adsorbent should have large capacity, fast adsorption rate, facile separation from water and easy regeneration (reactivate adsorption capacity by desorption) (Fu and Wang 2011). In the past decade, nanofibrous membrane (or mat in some cases) by electrospinning emerges as a new type of adsorbent. The membranes could be used either solely as adsorbents or in a membrane separation mode. With the latter, the characteristics of a separation by membrane make the process for metal recovery more continuous. Polymers dominate the materials used for producing nanofibrous membrane by electrospinning. With appropriate adjustment of material and fabrication, large specific surface area and high porosity could be delivered, which satisfies the thermodynamic and kinetic requirements in adsorption separation (Wang

✉ Lanying Jiang
jianglanyingsme@csu.edu.cn

1 School of Metallurgy and Environment, Central South University, Changsha 410083, Hunan, China

2 National Engineering Research Center for Control and Treatment of Heavy Metal Pollution, Changsha, China

3 Key Laboratory of Hunan Province for Water Environment and Agriculture Product Safety, Changsha 410000, China

et al. 2018). The PAA/SA nanofibrous membranes exhibited a maximum adsorption capacity up to 591.7 mg/g. Compared with powder or particle adsorbents, the assembly in a membrane structure ensures easier detachment from water. Moreover, high degree of adsorbent regeneration and metal recovery has been reported for some nanofibrous membranes in a relatively easy manner (Hong et al. 2015; Zhang et al. 2019). These points are meaningful in terms of both metal resource sustainability and waste reduction. Many conventional adsorbents are not separable and/or regenerable; they become heavy metal laden solid waste after utilization and their disposal commonly involves high cost (Sethurajan et al. 2018). Obviously, nanofibrous membranes have a big potential for heavy metal treatment.

In spite of the achievement in separation performance, large-scale implementation of nanofibrous membrane is challenged by inferior mechanical durability (Huang et al. 2013). This is firstly attributed to several factors in the process of spinning, including material intrinsic property (Al-Saleh and Sundararaj 2011), fiber arrangement (Hou et al. 2005), inter-fiber fusion and inter-molecular interaction, etc. (Obaid et al. 2016). The potential solutions to these problems are summarized in several researches and reviews (Pereao et al. 2019). Another more critical aspect is the post-treatment by chemical modification to give the membrane customized functionality on fiber surface (Pereao et al. 2019; DAISUKE ISHIMURA, Y.M.A.H. 1998). Kim et al. treated polyacrylonitrile (PAN) fibers by plasma to generate functional groups such as –COOH and –COOR in research about PM 2.5 removal. The fibers collapsed when the duration of modification exceeds 120 s (Kim et al. 1996). Hydroxide sulfonyl groups (–SO_3H) have the capacity for ion exchange. Kwak's research showed that polyethersulfone (PES) fiber mats were destroyed when sulfonation lasted for more than 150 min (Kwak et al. 2013). Yet another chemical group that has been followed with great interest is amidoxime (AO), one of the most effective structure toward chelating a wide group of metal ions (e.g., U^{6+}, Pb^{2+}, Cd^{2+}, Cu^{2+}) (Aguila et al. 2019; Yin et al. 2018; Zheng et al. 2019; Ren et al. 2018). It is generally formed by reaction between nitrile groups and hydroxylamine (NH_2OH). Khalid et al. prepared the AO-containing PAN nanofibers and found that the flexibility of the nanofiber mats decreased as the nitrile conversion increased (Saeed et al. 2008). Similar finding was reported in some other works (Neghlani et al. 2011). Mats contraction in size with high degree of AO formation (> 45%) was also observed (Neghlani et al. 2011). The reason for the above structural change or even deterioration of nanofiber is that the various chemical reactions originally targeting surface adjustment may cause irreversible change to the overall fiber if the reaction agents penetrates into the deeper part (Sagitha et al. 2018). Consequently, there is a compromise between separation performance and mechanical stability upon chemical modification.

In recent years, coaxial electrospinning to prepare fibers with composite core–shell structure receives much attention in catalysis, energy, filtration, tissue engineering, pharmaceutical, etc. (Qu et al. 2013). As compared with integral structure, the composite one can fulfill more diversified purpose by material selection and additional control. In Li et al.'s work, ultra-thin shells were designed for enhancing the fast dissolution of poorly water-soluble drugs (Li et al. 2018). Removing the core layer by an extraction process delivered hollow nanofibers exhibiting good performance in filtration and lithium ion batteries (Aslan et al. 2016; Li et al. 2017). The coaxial electrospinning was used to protect glucosamine sulfate (GAS) from environment by the outer polycaprolactone (PCL) layer, so as to control drug release over time (Chen et al. 2020). The technology has also been adopted for tackling the typical conductivity–strength trade-off of proton exchange membrane (PEM). Key to the breakthrough is the enhanced fiber strength by extra electrostatic force provided by the inner nozzle wall (Yuan et al. 2020). As far as coaxial operation is concerned, it presents as a more convenient alternative to multi-step fabrication targeting similarly the composite structure (Qu et al. 2013).

In current work, flexible PAN nanofibrous membranes with AO functionality were prepared for treating heavy metals by adsorption. The fibers were designed with core–shell structure and fabricated by coaxial electrospinning. AO groups were introduced by reaction of PAN in shell layer with NH_2OH, as mentioned above (Saeed et al. 2008). The desired flexibility relies on the core layer made from PVDF. This is a polymer that has excellent chemical stability in many environments and is expected to maintain structural integrity during PAN chemical modification (Graphical Abstract). The nanofibrous membranes fabricated were tested in adsorption and filtration for Pb^{2+}, a possibly carcinogenic chemical. The tensile characterization was conducted to confirm to what degree the PAN/PVDF composite nanofibrous membrane can maintain the flexibility and strength during chemical modification and regeneration.

Experimental

Materials

N, N-Dimethylacetamide (DMAc, AR reagent, ≥ 99.5%), polyacrylonitrile (PAN) with a weight-average molecular weight (Mw) of 150,000 $g \cdot mol^{-1}$ and hydroxylamine hydrochloride ($NH_2OH \cdot HCl$) were bought from Sinopharm Chemical Reagent Co. Ltd. (China). Poly(vinylidene fluoride) (PVDF) with a weight-average molecular weight (Mw) of 350,000 $g \cdot mol^{-1}$ was bought from Kureha Chemical

Industries (Osaka, Japan). Lead nitrate $Pb(NO_3)_2$ was purchased from Tianjin Kemiou Chemical Reagent Co. Ltd. (China). Sodium carbonate (Na_2CO_3) was obtained from Hunan Huihong Reagent Co. Ltd. Hydrochloric acid (HCl) was purchased from Chengdu Chron Chemicals Co. Ltd. All chemicals were used as purchased.

Preparation of membranes with core–shell nanofibers

PAN and PVDF powders were vacuum-dried at 120 °C overnight before dope preparations. They were, respectively, added into DMAc solvent and mixed by magnetic stirrer at 60 °C for 4 h, until a homogeneous solution is formed. Place the solution at room temperature until the bubbles are removed; PAN and PVDF solutions of different concentrations were transferred into two 10-mL syringes, respectively, which were then connected to coaxial needles through a polytetrafluoroethylene (PTFE) tube. The nanofibers were fabricated by electrospinning device (JDF04, Changsha Nano Instrument Technology Co., Ltd, China) at a flow rate of 0.5/0.5 mL/h for 2 h. The needle is fixed 15 cm above the roller; the diameter and length of the roller are 92 mm and 19.5 cm, respectively, and the rotation speed is 300 rpm. The temperature and relative humidity during electrospinning were 25 °C and 55%, respectively. After fabrication, the membrane was placed in oven at 60 °C for removing the residual solvent.

Chemical modification

The outer PAN was chemically modified to generate amidoxime chelating group, and the reaction mechanism is given in Fig. 1a. The modification was carried out by hydrothermal method. Solutions with different ratio of anhydrous sodium carbonate (Na_2CO_3) and hydroxylamine hydrochloride ($NH_2OH{\cdot}HCl$) (prepared by dissolving NH_2OH in acid) were added to 100 mL deionized (DI) water at 70 °C, followed with immersing the membrane into the solution for the modification. The membranes attached to non-woven support temporarily were fixed by clamps to prevent shrinkage. The membranes after modification were symbolized AOPAN/PVDF and rinsed by deionized water for three times to removal residual chemicals. The AOPAN/PVDF membrane was then freeze-dried under vacuum.

Adsorption and regeneration experiments

The static adsorption experiments were carried out in well-sealed blue cap bottles, each of which contained 50 mL aqueous solution of $Pb(NO_3)_2$ at 200 mg/L with the membrane dosage of 100 mg/L and was shaken for 24 h. To analyze the pH effect, solutions with concentrations of 200 mg/L and the pH values of the solution were adjusted from 2 to 5 by HCl and NaOH. For regeneration study, the AOPAN/PVDF nanofibrous membranes were first equilibrated with Pb^{2+} in solution at concentration of 200 mg/L for XX hours; the membrane was then taken out and removed of residual liquid. Thereafter, the AOPAN/PVDF membranes was immersed into 50 mL 0.1 M HCl for 1 h.

The Pb^{2+} concentration of solutions before and after adsorption were determined. The amount of Pb^{2+} ions adsorbed on the membrane (mg/g) was calculated by the following equation (Habiba et al. 2017; Dognani et al. 2019):

$$q_e = \frac{(C_0 - C_e)V}{m} \quad (1)$$

where q_e is the amount of Pb^{2+} adsorbed (mg/g), C_0 and C_e is the initial and the equilibrium Pb^{2+} ions concentration (mg/L), respectively, V is the solution volume (L), and m is the amount of membrane used (g).

In the flow-through test, the dynamic adsorption was performed on a dead-end filtration setup using a single-pass flow with pH = 5 (Fig. 1b). The setup consists of a peristaltic pump (BT-600EA, JIHPUMP, China) and a circular sand core support with an active diameter of 4 cm. The filtrates were sampled at a definite interval. The dynamic adsorption

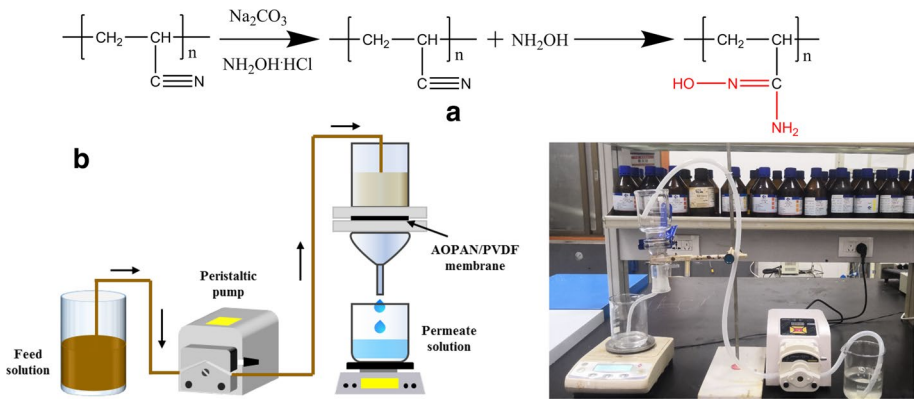

Fig. 1 Routes for **a** PAN nitrile conversion to amidoxime and **b** the schematic and picture of the membrane filtration setup

rate (v_t) at different time was determined by following equation (Fan et al. 2019):

$$v_t = \left(C_0 - C_t\right)v \tag{2}$$

where v_t (mg/min) was the adsorption rate at time t (min); C_0 (mg/mL) was the initial concentrations of Pb^{2+} solution; C_t (mg/mL) was the concentration of the filtrate at time t; v (mL/min) was the flow rate.

The dynamic adsorption capacity per unit membrane area (q_d) was calculated by was calculated by following equation (Fan et al. 2019):

$$q_d = \frac{q_e'}{A} \tag{3}$$

where q_d (mg/cm) was the adsorption capacity per unit area of the membrane; q_e' (mg) was the total adsorption capacity of the membrane, which is equal to the area under v_t-t curve; A (cm^2) is effective area of the membrane.

The concentration of Pb^{2+} in aqueous solution was measured by inductively coupled plasma–atomic emission spectroscopy (Agilent Technologies, ICP-5100-VDV, Malaysia). The data were used for the calculation in Eqs. (1–3).

Other characterization

The morphology of the membranes was analyzed by double beam electron microscope (FESEM, Helios Nanolab G3 UC, Czech). The diameter of fibers was measured by software ImageJ. Chemical structure of the membranes was characterized by Fourier transform infrared spectrometer (FTIR) (Bruker, TENSOR27, USA). The Mechanical strength test of the membrane was performed with a commercial test machine (WDW-100 N, Jilin Tanhor Testing Machine). The TEM images were observed by spherical aberration transmission electron microscope (FEI, Titan G2 60–300, USA). The specific surface area was measured at 77 K with a liquid nitrogen bath and analyzed using Quadrasorb SI-3MP (Quantachrome, Quadrasorb SI-3MP, USA). The wide-angle X-ray diffraction (WAXD) patterns were detected by an X-ray diffractometer (West Germany's Siemens Company, D500, Germany). Membrane thermal stability was tested by thermogravimetry–differential scanning calorimetry (TG-DSC) (Netzsch Instruments Manufacturing Co., Ltd., NETZSCH STA 449F3, Germany).

Result and discussion

Preparation of core–shell fiber membrane

In electrospinning, the polymer solution is pumped out of the needle at a constant speed, overcoming the surface tension by internal charge repulsion and external electrostatic force and stretching to form nanofibers[39]. The physical properties of the nanofibers are influenced by several factors, such as polymer concentration, operation voltage, temperature and humidity (Drosou et al. 2018).

In electrospinning process, the voltage adopted is very critical for achieving solution stretching to form fibers. Only when attaining threshold and higher voltage can the fibers be developed. Researchers have some different views about the influence of the voltage in electrospinning. Zhang et al. suggested that the volume ejection rate for polymer solution was higher at high voltage, which promotes the formation of fibers with larger diameter (Zhang et al. 2005). More works found that a higher voltage generated higher degree of polymer solution stretching due to a stronger electric field and hence delivered smaller fiber diameter (Bhardwaj and Kundu 2010). We used a camera to observe the process characteristics of the coaxial electrospinning (vedio1-3). Confirmed by TEM pictures is that both voltages of 13 and 14 kV can lead to the formation of a core–shell structure. As can be seen from Fig. 2 a1–a3 of the pictures captured from the videos, the linear regions of the ejected fibers were stable and regular at 13 and 14 kV. When the voltage reached 15 kV, two jet streams appeared between the tip and collector, as shown in the red circles in Fig. 2-a3. Multi-ejection at high voltage has been reported by some researches (Zanjani and J, Saner Okan B, Letofsky-Papst I, Yildiz M, Menceloglu YZ 2015). Another possible reason in current work is that the two solutions respond to charge and electrostatic field in different manner. When voltage is high (i.e., 15 kV), the difference might be big enough to allow their peeling off from each other after extrusion. As result, approximately single-layer fiber structure was formed, as shown by TEM (Fig. 2-c3). The problem with 13 kV is that some bead-on-string phenomenon occurs, as shown in Fig. 2-c1. The fibers connected with beads were thinner, which might collapse easily when subject to mechanical stress (Wang et al. 2020). Lower applied voltage results in weaker electrostatic attraction between the needle tip and the collector, generating lower drawing stress in the jet, which leads to the polymer solution aggregation in the needle tip (Fig. 2-a1). This is the major mechanism for the bead development (Lee et al. 2003). It has been revealed in some researches that higher voltage brought about unstable and unpredictable, which formed multiple jet flow during electrospinning process. Therefore, 14 kV was the most suitable voltage for the coaxial electrospinning.

The effect of polymers concentration on core–shell fibers morphology were studied in this work and different combinations of PAN concentration in outer layer and PVDF concentration in inner layer were selected, as shown in Table 1. It was found that when the concentrations of solutions for both inner and outer layers were lower than 10 wt%, there existed fiber disruption and bead formation. Raising polymer

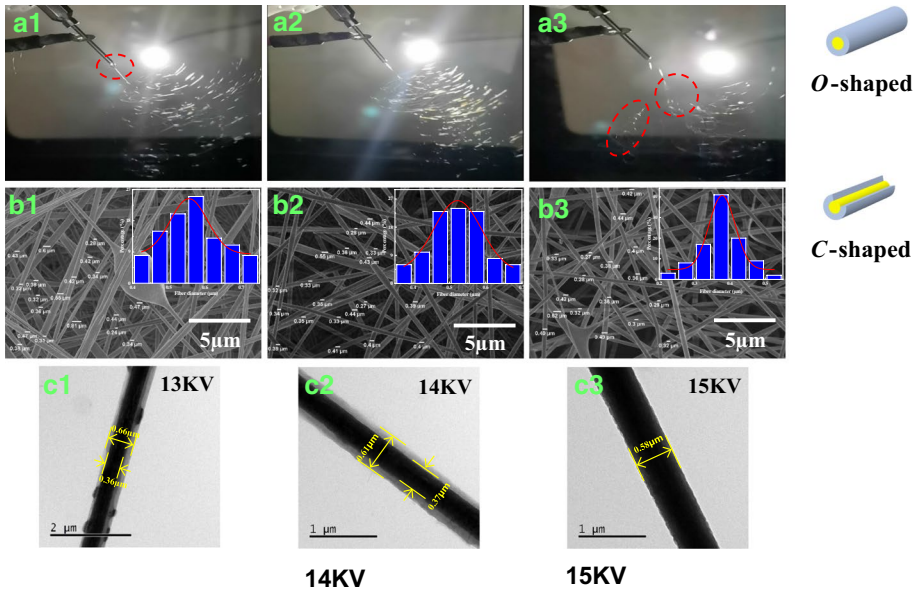

Fig. 2 **a** The optical images during the electrospun process, **b** the SEM images and **c** the TEM images of the fibers at different voltages

Table 1 Effect of PAN and PVDF's concentration on the diameter and integrity of the nanofibers

PAN (Shell)	PVDF (Core)	Diameter distribution (ii m)	Mean diameter (*v*- m)	Bead number	Integrity
10%	6%	0.091 + 0.045	0.075	Many	Break
	8%	0.128 + 0.076	0.093	Many	C-shaped
	10%	0.173 + 0.099	0.152	Few	C-shaped
	12%	0.206 + 0.097	0.167	Very few	C-shaped
12%	6%	0.162 + 0.075	0.155	Very few	O-shaped
	8%	0.180 + 0.069	0.164	Very few	O-shaped
	10%	0.189 + 0.099	0.185	No	O-shaped
	12%	0.235 + 0.079	0.244	No	O-shaped
14%	6%	0.268 + 0.136	0.252	Very few	O-shaped
	8%	0.323 + 0.111	0.305	Very few	O-shaped
	10%	0.271 + 0.087	0.267	No	O-shaped
	12%	0.334 + 0.129	0.329	No	*O*-shaped

concentration increased the spinnability; larger and more uniform diameter of fibers and reduced number of bead-on-string phenomenon were resulted with higher concentration. This observation is consistent with that reported in Fong et al.'s and Chen and Jiang's research (Fong et al. 1999; Chen and Jiang 2020). The diameter change was believed to be related to the increase in the solution viscosity (Dong et al. 2004). Nonetheless, higher viscosity will enhance the propensity of needle clogging during electrospinning. Observed was also the dependence of the integrity of the dual-layer structure on solution concentration. As shown in Fig. 3 a2-a4, some fibers exhibit a cross section with an incomplete outer layer (*C*-shaped). Additional phases introduce an interface interaction (miscibility and stress due to the viscosity difference), and the individual physical behavior of different phases (solidi cation and conductivity) also complicates the coaxial electrospinning (Qu et al. 2013). When the concentration of the outer solution is low, the polymer chain entanglement was not sufficient to generate continuous thinning and deposition that can cover fully the core layer. On the other hand, an insufficient core solution cannot support a continuous smooth core phase (Ou et al. 2011). In other words, the concentrations of both layers are critical for obtaining a uniform and complete morphology.

The mechanical strength of different fiber membrane was characterized by a commercial test machine (WDW-100 N, Jilin Tanhor Testing Machine), and the results are displayed in Fig. 4. It was shown that increasing the concentration of PVDF in the inner layer improved the mechanical strength of the nanofibrous membrane, and the relationship is approximately linear. As discussed in the above section, the core–shell fibers attained bigger diameter with higher

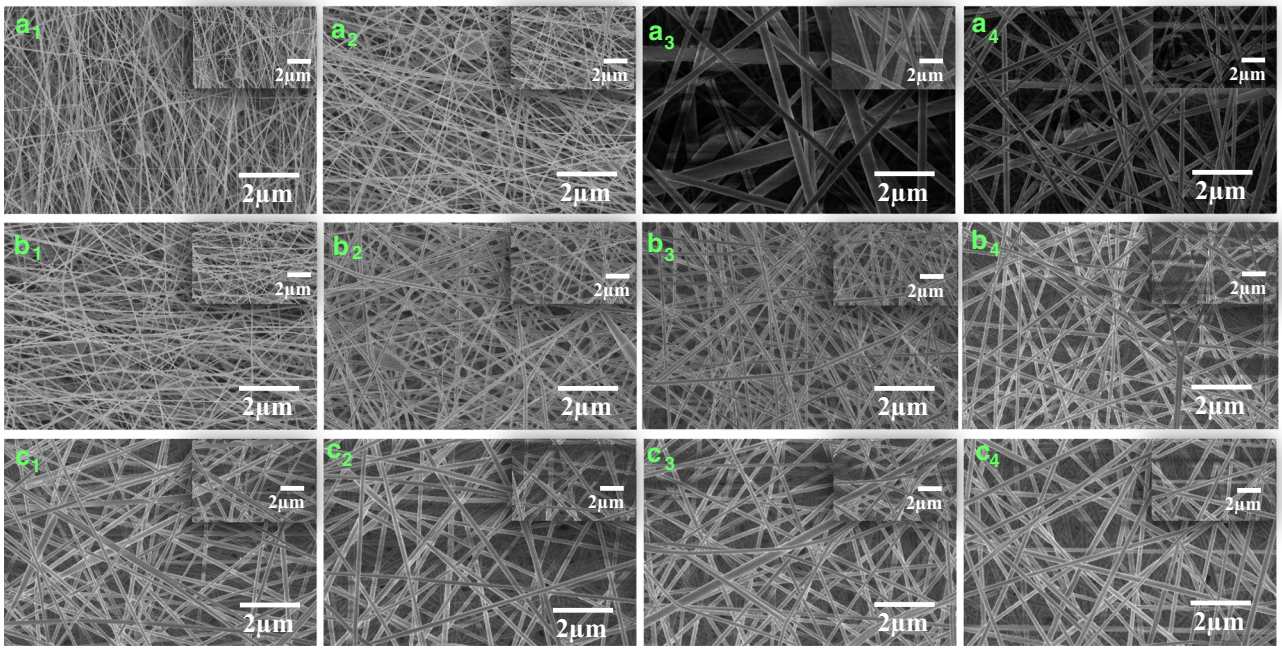

Fig. 3 SEM images of electrospun fibers:. a1–a4 10% PAN inner layer 6–12% PVDF, b1–b4 outer layer 12% PAN inner layer 6–12% PVDF, c1–c4 outer layer 14% PAN inner layer 6–12% PVDF

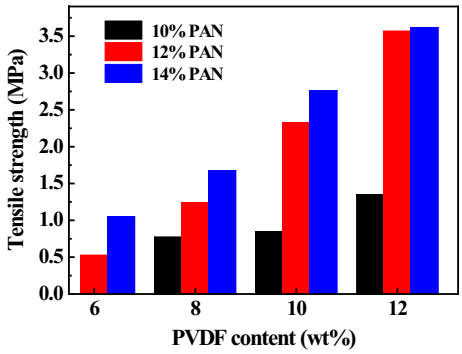

Fig. 4 The tensile strength of nanofibrous membrane fabricated from different PAN and PVDF solutions

polymer concentration (Table 1). The change in the diameter is one of the factors underlying the variation in mechanical strength (Wang et al. 2020). For membranes using a concentration in the range of 10–6%, the strength of the membrane is too low to be accurately analyzed. Also revealed in Fig. 4 is the change in mechanical strength with PAN concentration at fixed PVDF concentration. When PVDF concentration was equal and lower than 8 wt% and PAN is 10%, the fibers could not be formed. For PVDF at 10 and 12%, an abrupt enhancement followed by a mild increase as PAN content changed from 10 to 14%. The mechanical strength of the core–shell fiber depends on both layers. When PAN is at low level, the outer layer is not complete (i.e., *C*-shape indicated in Fig. 2), which presents as defects for the overall structure. For fibers with completeness in outer layer, the slight increase in the mechanical strength with PAN content might be due to the minor proportion of the outer layer in the overall structure. Taking structural integrity and mechanical strength as the major standard, the 12 wt% (outer)-12% (inner) combination was selected for the following chemical modification.

The effect of chemical modification on core–shell fibers

The PVDF/PAN core–shell fibers were treated by hydrothermal method to obtain amidoxime functional groups (the reaction route is shown in Fig. 1a). Our preliminary experiment showed that 70 °C was appropriate for the amidoxime formation. The reaction rate slows down with the temperature drops, while at higher temperature the membrane will shrink seriously. The reactants played an important role as well in the conversion rate of nitrile groups and we investigated three different ratios of hydroxylamine hydrochloride ($NH_2OH{\cdot}HCl$) and Na_2CO_3.

The concentration of amidoxime group in the core–shell fibers is calculated by the following formula (Saeed et al. 2008):

$$C_a = \frac{W_1 - W_0}{M_1 \times \left[W_0/2 + \left(W_1 - W_0\right)\right]} \times 1000(\text{mmol/g}) \quad (4)$$

where W_0 (g) is the mass of nanofiber mat before reaction; W_1 (g) is the mass of nanofiber mat after reaction; M_1 is the molecular weight of hydroxylamine (33 g/mol).

The reaction rate constant can be obtained by using the content of amidoxime group at different hydroxylamine concentrations. The equation is as follows (Alakhras et al. 2005):

$$\ln V = \ln\left(-\frac{dC_i}{dt}\right) = n \ln C_i + \ln K \tag{5}$$

where V (mmol/s) is the reaction rate; C_i is the component concentration at time i (mol/L); t is time; n is the reaction order; K is the reaction rate constant.

The value of K is estimated from the intercept of the straight curve shown in Fig. 5, and the other parameters in Eq. (5) are given in Table 2. The excess of both reactants hindered amidoxime formation. When Na_2CO_3 was excessive, the reaction rate decreased obviously. Higher content of Na_2CO_3 increases the pH of the solution and reduces the amount of free hydroxylamine ions (NH_2OH).

For the pure PAN fibrous membranes, the fibers became very brittle when the conversion rate of nitrile group is over 35% (Saeed et al. 2008). The conversion rate of amino indicates the degree of amidoxime formation reaction and is calculated by following equation (Saeed et al. 2008):

$$C_n = \frac{\Delta M}{M_0/2}\frac{W_0}{W_1} \times 100\% \tag{6}$$

where C_n (%) is the conversion rate of nitrile group in PAN into amidoxime group; ΔM (g) is the mass of core–shell nanofiber mat difference before and after reaction; M_0 (g) is the mass of the core–shell nanofiber mat before reaction; W_0 is the molecular weight of acrylonitrile monomer (53 g/mol); and W_1 is the molecular weight of hydroxylamine (33 g/mol).

The different conversion degrees for nitrile group were further confirmed by FTIR (Fig. 6a). The adsorption peak at

Table 2 The reaction rate constants of amidoximation at different ratios of hydroxylamine hydrochloride and sodium carbonate

NH_3OHHCl (mol): Na_2CO_3 (mol)	Temperature (°C)	Time (min)	pH	K
2:1	70	60	6.04	4.74×10^{-3}
2.5:1	70	60	5.73	2.51×10^{-3}
1:1	70	60	8.80	7.27×10^{-4}

2250 cm^{-1} was assigned to the –CN group stretching vibration, and the peak intensity decreased as the conversion of the nitrile to the amidoxime group increased (Puspitasari et al. 2018); the peak of C=O in ester at 1730 cm^{-1} was reduced due to the introduction of hydroxamic acid groups (Alakhras et al. 2005); the observed absorption band at 1650 cm^{-1} in curses were attributed to the stretching of C=N (Hu et al. 2016).

The XRD patterns of AOPAN/PVDF nanofibers are shown in Fig. 6b. There had a sharp peak at around 21.4°, which corresponds to the PVDF molecular chains (Sun et al. 2020). The characteristic peak at 23.8° and 26.5° is commonly observed with PAN fibers (Feng et al. 2020). The result shows that the crystallinity of the core–shell nanofibers had been largely retained with different AO conversion. This provides a validation for the strength retention of core–shell fibers.

The thermal stability of PAN/PVDF and AOPAN/PVDF core–shell nanofibers is displayed in Fig. 6c-d. The curve of PAN/PVDF had three step changes in mass with temperature increase, which occurred at 70, 250 and 400 °C, respectively. The curves for AO modified fibers also exhibited three major step change, but with the second being obviously lower. The weight loss happening at the temperature range from 50 °C to around 150 °C are generally ascribed to evaporation of moisture. And the change at temperature higher than 320 °C are supposed to be related with original polymer chain including both PAN and PVDF. Therefore,

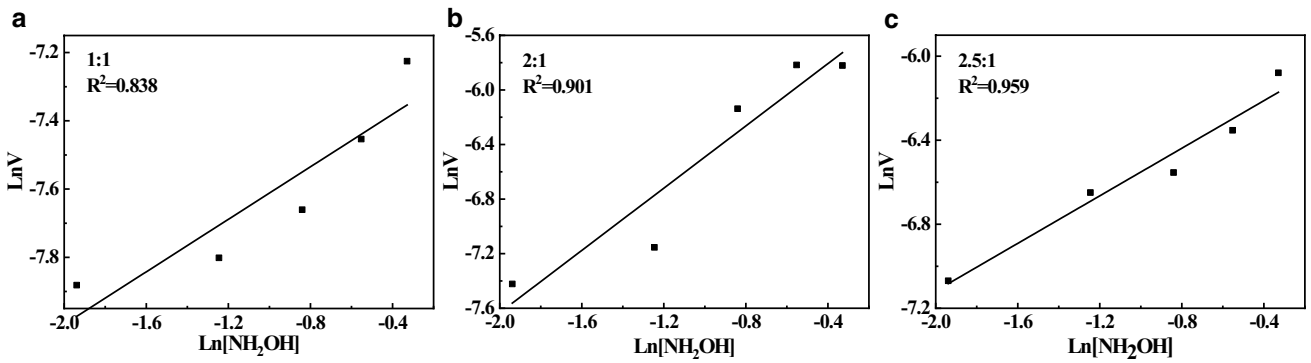

Fig. 5 Logarithmic diagram of the reaction rate as a function of the ratio of reactants (**a** 1:1, **b** 2:1, **c** 2.5:1)

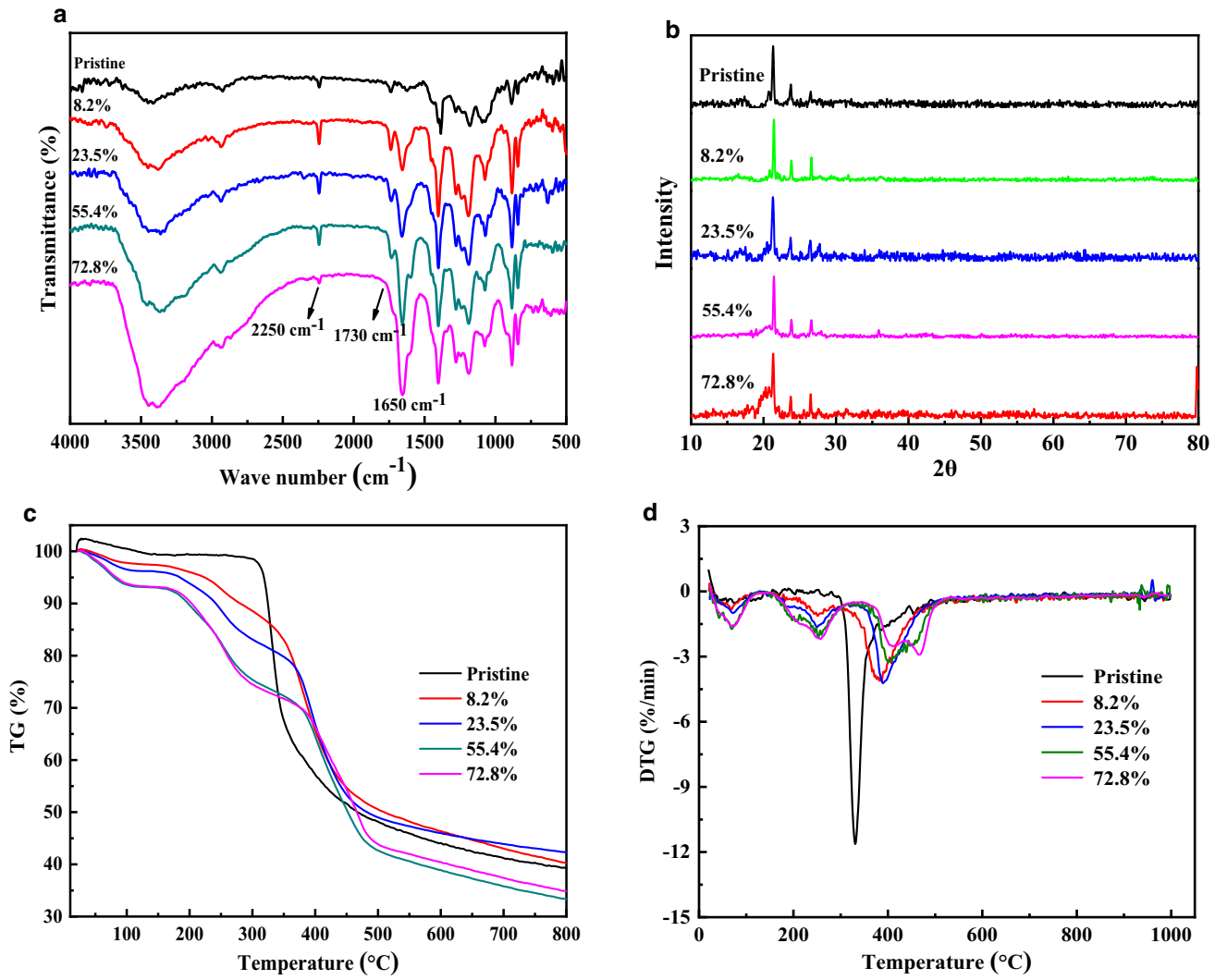

Fig. 6 **a** FTIR spectra, **b** XRD patterns, **c** TGA curves and **d** DTG curves of AOPAN/PVDF nanofibrous membranes with different nitrile group conversion

this indicated AOPAN/PVDF fibers still retained part of its structure unchanged in amidoxime modification (Blend-electrospun poly(vinylidene fluoride)). The difference in the second inflection point implies that the thermal stability of the modified fibers degraded. This is thought due to the decomposition of the amidoxime groups.

The mechanical strength of neat PVDF and AOPAN/PVDF fiber mats with different conversion rates are shown in Table 3. The neat PVDF nanofiber membrane was prepared by 12% PVDF dope solution at 14 kV voltage for 2 h. After being treated by hydroxilamine at 70 °C, the mechanical strength of neat PVDF fiber is slightly improved, which could be used as a proof for the chemical stability for PVDF in the reaction. The reason behind the improvement may be the thermal annealing that rearrange the polymer chain packing. Both tensile strength and tensile elongation decreased

Table 3 Mechanical strength and softness of the neat PVDF and AOPAN/PVDF nanofiber membranes at the different conversion of nitrile groups

Conversion rate	Tensile strength (MPa)	Tensile elongation	Flexibility
PVDF	3.775	23.735	soft
PVDF after amidoxime	4.112	17.423	soft
Pristine (0%)	3.567	32.067	Soft
8.2%	2.769	27.934	Soft
23.5%	2.794	29.546	Soft
55.4%	3.016	27.6	Soft
72.8%	2.852	10.819	Soft

with increase in conversion degree, but core–shell nanofibers with a conversion rate of 72.8% maintained much of its original morphology according to SEM image (Fig. 7). Bending tests also showed that the nanofibrous membrane have durable flexibility. The mechanical strength of nanofiber reported in other literature is shown in Table 4, and the property of the fibers by current work is better than that in most of the other researches. The specific surface area was 5.813 m^2/g. Therefore, AOPAN/PVDF obtained from core–shell electrospinning is a promising material for water treatment.

Adsorption performance

Static adsorption

The reaction mechanism for amidoxine group is given in Fig. 8. The effect of the initial pH on the adsorption capacity of the AOPAN/PVDF nanofibers mats for the same Pb^{2+} is summarized in Fig. 9a. The time duration for all the tests was set at 24 h, to ensure the adsorption equilibrium was attained. The results showed that the adsorption capacity

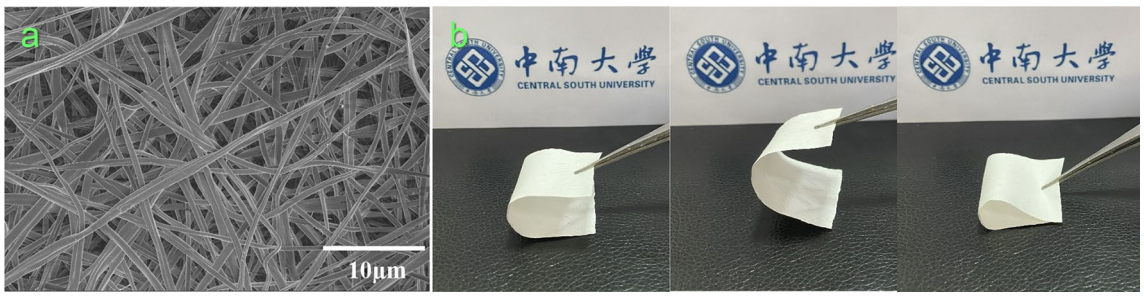

Fig. 7 **a** SEM image and **b** optical images demonstrating flexibility of the AOPAN/PVDF nanofibers (70 °C and 120 min)

Table 4 Comparison of the mechanical properties and diameters from different researches

Polymer	Electrospinning method	Mechanical properties			Reference
		Strength (MPa)	Strain (%)	Diameter (nm)	
CA/PAN	Multi-fluid	1.4 – 5.1	14.8 – 29.2	303 – 502	Wang et al. 2020)
CA/PAN	Multi-layering	1.6	109.8	280 – 404	Karki et al. 2019)
CA/PAN	Blending	1 – 3	50 – 75	150 – 200	Bui and McCutcheon 2013)
MOFs/PAN	Blending	3 – 5.1	–	148 – 254	Li et al. 2020)
AOPAN	–	1.26	12	80 – 330	Zhijiang et al. 2017)
Polysulfone (PSu)	–	0.77	–	–	Huang et al. 2013)
PVDF	–	1.7	47.2	–	Ding et al. 2019)
PVDF-SiO_2	Blending	3.8–5.5	187.5 – 375	200 – 900	Obaid et al. 2016)
PVDF/CNT	Blending	4.2	49.1	138 – 156	Wu and Chou 2016)
AOPAN/PVDF	Coaxial	3.57	32.1	235 – 314	This study

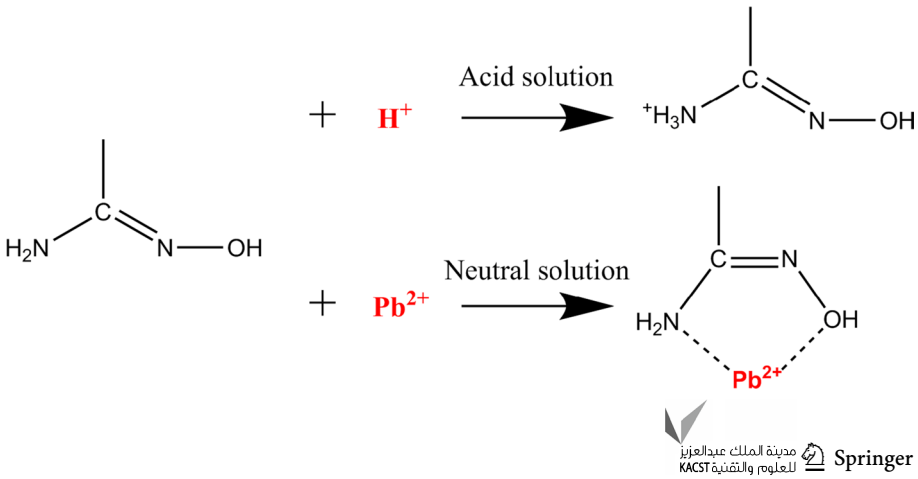

Fig. 8 The reaction of AOPAN/PVDF in water at different pH values

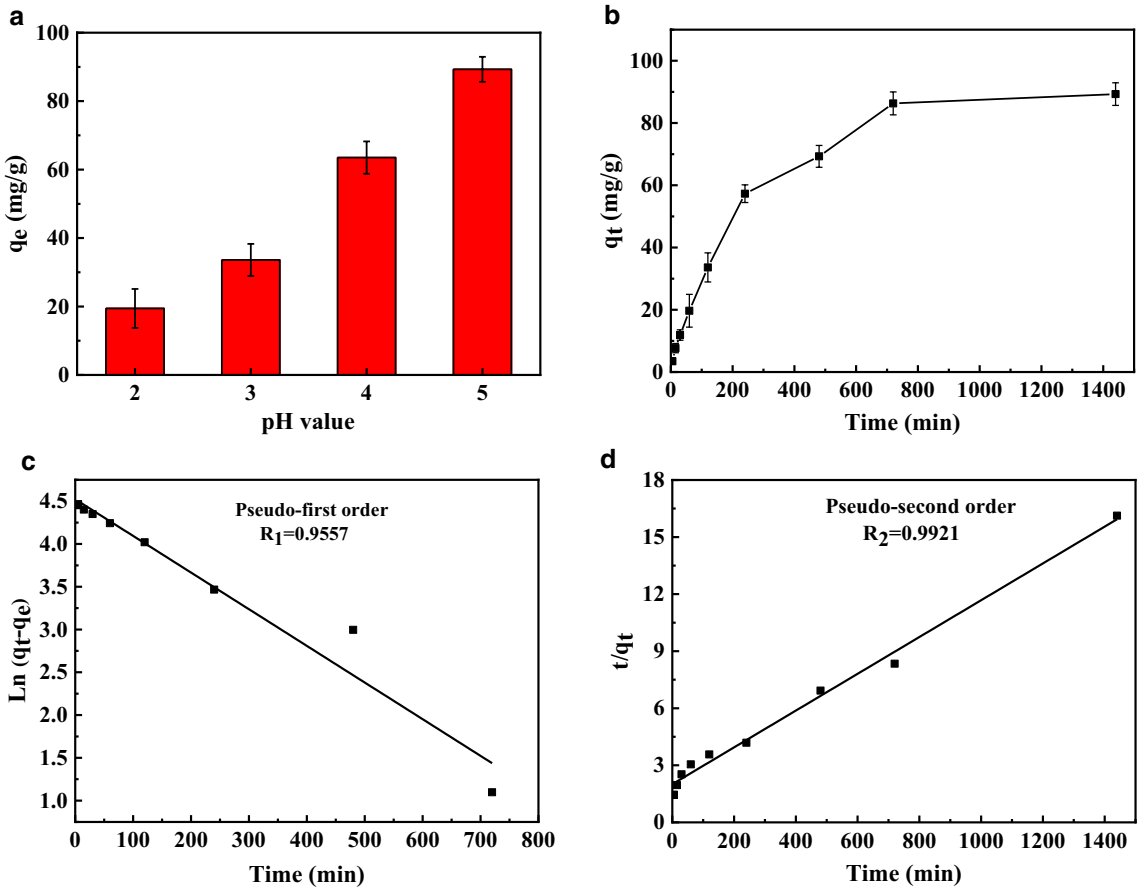

Fig. 9 **a** The effect of pH on the Pb2 + adsorption capacity, **b** the effect of the contact time on the adsorption of Pb2 + and (**c**1-2) the adsorption kinetic modeling using a pseudo first-order and pseudo second-order models

of Pb^{2+} on AOPAN/PVDF core–shell fibers increased with the increase of pH value. And the adsorption capacity was very low at pH = 2. This was first attributed to the competition between Pb^{2+} and H^{+} toward the adsorption site. Additionally, the electrostatic repulsion from protonated amino was higher for Pb^{2+} than H^{+}; the former has larger diameter and higher valence. Therefore, it is difficult for Pb^{2+} to approach and adhere to the functional group of AOPAN/PVDF core–shell fibers (Hong et al. 2015). When the pH is above 5, the Pb^{2+} would precipitate in the form of $Pb(OH)_2$ and $PbCO_3$, which affects greatly its adsorption behavior. The Pb^{2+} adsorption performance compared to other adsorbents is summarized in Table 5. The maximum adsorption capacity of AOPAN/PVDF for Pb^{2+} is 89.29 mg/g, which is higher than part of the other nanomaterials. It is expected to be a new material for Pb^{2+} removal from water.

Figure 9b shows the adsorption amount of Pb^{2+} on the AOPAN/PVDF core–shell fibers as a function of the contact time (pH = 5). The capacity increased with an increase of the contact time. The equilibrium adsorption capacity of Pb^{2+} on the AOPAN/PVDF core–shell fibers were reached within 12 h. Adsorption kinetics can be employed to describe the

Table 5 Comparison to other materials for Pb^{2} + adsorption

Material	Adsorption capacity (mg/g)	Reference
P -CD/CS/PVA nanofiber membrane	37.1	Fan et al. 2019)
PVA/PAA nanofibers	159	Zhang et al. 2019)
MWCNTs	7.2	Efome et al. 2018)
Mg_2Al LDH	60.98	Anirudhan et al. 2019)
Pb (II) imprinted chitosan	79.2	Xiao et al. 2019)
Pb (II)-IIP	97.5	Wang et al. 2007)
AOPAN/PVDF	89.29	This study

adsorption rate and possible adsorption mechanism. Pseudo first-order and pseudo second-order models were used to analyze the nature of the kinetics and the rate of Pb^{2+} adsorption by the AOPAN/PVDF membrane. The linear forms of these two models are fitted by following equations, respectively (Zhao et al. 2011).

$$\ln\left(q_e - q_t\right) = \ln q_e - k_1 t \tag{7}$$

$$\frac{t}{q_t} = \frac{1}{k_2 q_e^2} + \frac{1}{q_e} t \tag{8}$$

where q_e ($g{\cdot}g^{-1}$) is the equilibrium adsorption capacity, q_t ($g{\cdot}g^{-1}$) is the amount of metal ions adsorbed at time t, t (min) is the duration of the adsorption, k_1 (min^{-1}) and k_2 ($g{\cdot}g^{-1}\ min^{-1}$) are the first- and second-order rate constants, respectively.

The best fit model was selected based on linear regression correlation coefficient (R^2). According to Fig. 9c, pseudo second-order model ($R^2 = 0.9921$) showed a better fit with the experimental data than pseudo first-order model ($R^2 = 0.9557$). The basic assumption of pseudo second-order model is that the adsorption process is major in chemical adsorption. Many researchers have reported the similar mechanism (Lu et al. 2013; Zhu et al. 2016). The deprotonation of -NH_2 and -OH on amidoxime group can be chelated with Pb^{2+} in liquid, which is the main mechanism of Pb^{2+} adsorption by AOPAN/PVDF (Zhuang et al. 2018).

The FTIR spectra of AOPAN/PVDF and after adsorption are shown in Fig. 10a; it is found that new peaks appear at 1598 and 1528 cm^{-1} after adsorption, which is related to the affinity binding with Pb^{2+} and also confirms that Pb^{2+} is adsorbed on the surface of AOPAN/PVDF (Hong et al. 2015). The membrane adsorption property and regeneration efficiency in five consecutive cycles is shown in Fig. 10b. It is revealed that the adsorption capacity of AOPAN/PVDF membranes decreased with each adsorption–desorption cycle. And the capacity became 44 mg/g in the adsorption at the 5th cycle. The Pb^{2+} on membrane could not be completely removed from the membrane during the desorption step; some lead ions permanently occupied the adsorption sites and the adsorption sites on membrane decreased with increasing repetitions (Ren et al. 2018). It should be noted that the mechanical strength of the AOPAN/PVDF membrane did not change significantly in the reuse process. This was attributed to the core–shell structure. The inner support layer avoids the collapse of the membrane during the modification process, so that the mechanical properties of the membrane can be maintained.

Flow-through adsorption

Dynamic adsorption in membrane filtration mode was performed on the dead-end filtration setup (Fig. 1b) using a single-pass flow. The filtrates were sampled at the set time, and the concentrations of Pb^{2+} ions in the samples were determined by ICP.

The Pb^{2+} adsorption for the AOPAN/PVDF membranes obtained at different filtration rates is presented in Fig. 11a. Obviously, the filtration rate had a significant influence on Pb^{2+} capture. For all the three tests, Pb^{2+} breakthrough happened almost immediately after the starting of the test. When the filtration rate was 2.66 mL/min, the concentration of Pb^{2+} in effluent increased sharply within 20 min. Higher filtration rate signifies that the residence time of the feed solution in the AOPAN/PVDF membrane may be too short, hence resulting in faster breakthrough. With higher initial concentration, the time required for Pb^{2+} to break through the membrane was very short, as shown in Fig. 11b. When the concentration was at lower level of 10 mg/L, Pb^{2+} concentration increase at the initial stage was milder (Fig. 11b). The dynamic adsorption rate v_t at different filtration rate and initial Pb^{2+} concentrations are summarized in Fig. 12. Table 6 displays the q_d of conditions which calculated by Fig. 12. It was observed that q_d increased and then decreased with the filtration rate. With a higher filtration rate, more amount of Pb^{2+} ions will pass through the membrane within the same period of filtration time; but ions may not have sufficient time to transport to the adsorption sites. If the latter factor overtakes the former, q_d will be reduced.

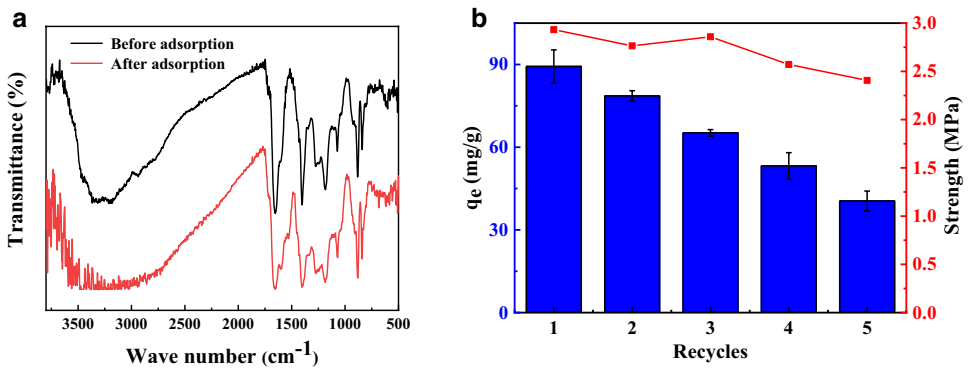

Fig. 10 **a** FTIR spectra of AOPAN/PVDF and after adsorption, **b** performance of the AOPAN/PVDF membrane (70 °C and 120 min) in five consecutive cycles of adsorption and regeneration

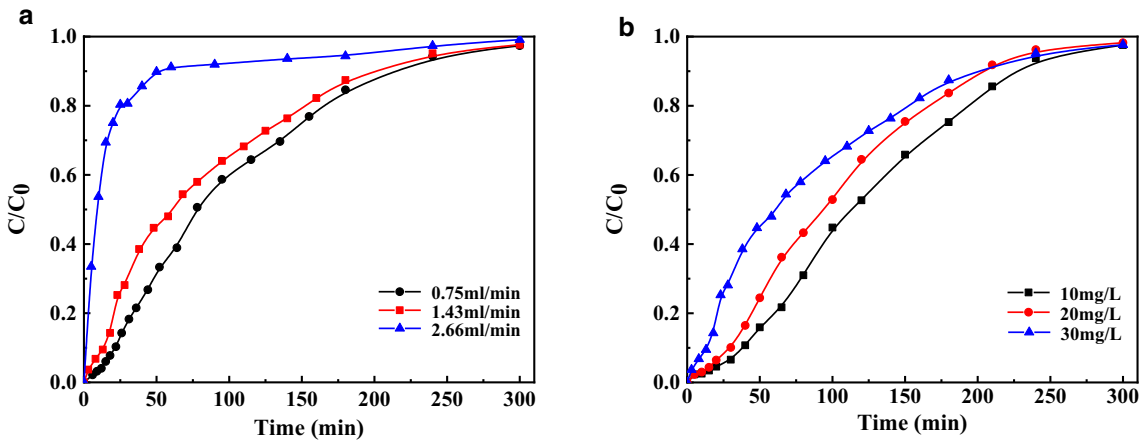

Fig. 11 Effect of feed flow rate **a** and Pb 2 + initial concentration **b** on dynamic adsorption for Pb2 +

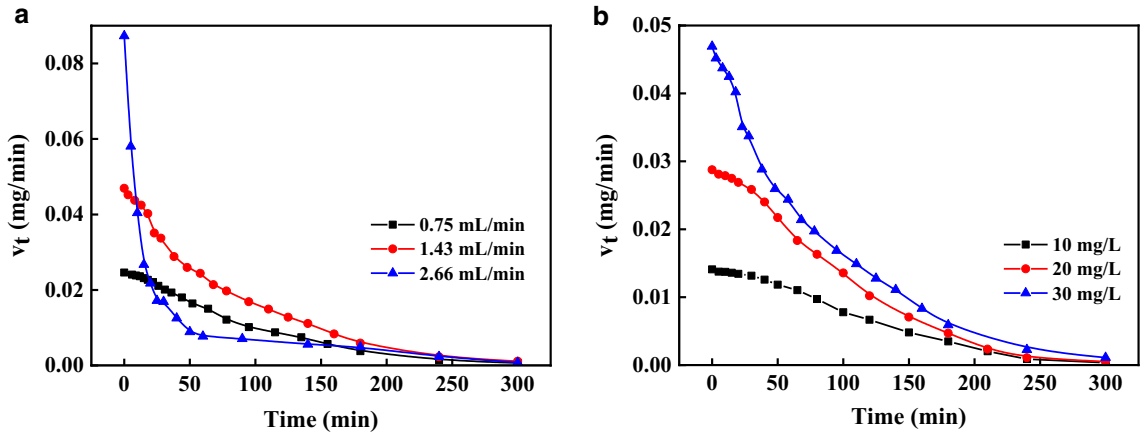

Fig. 12 The calculated *Vt* as function of *t* at different feed flow rates (**a**) and Pb2 + initial concentration (**b**)

Table 6 The dynamic adsorption capacity per unit area (Q_d) calculated using the data in Fig. 12

Conditions	Trans-membrane flow rate (mL/min)			Concentration (mg/L)		
	0.75	1.43	2.66	10	20	30
Q_d (mg/cm^{-2})	0.197	0.321	0.196	0.140	0.242	0.321

Conclusions

The core–shell PAN/PVDF nanofiber membrane was fabricated by coaxial electrospinning, and then modified by amidoxime. The applied voltage has a great influence on the process of electrospinning and the morphology of the fiber. The polymer solution cannot be fully stretched under 13KV, which caused bead-on-string phenomenon, while 15KV causes instability in the electrospinning process. Through fiber morphology and mechanical strength test, 12%PAN–12%PVDF is the most suitable polymer concentration ratio. The core–shell structure greatly enhances the stability of the fiber in amidoxime modification. The morphology and strength of the membrane are still preserved when the conversion of nitrile group in PAN was over 70%. The membrane has excellent removal performance on Pb^{2+}, and more importantly, its mechanical properties are stable during the regeneration process. The AOPAN/PVDF membrane can effectively retain Pb^{2+} in dynamic filtration, indicating the potential of the AOPAN/PVDF for industrial applications.

Supplementary Information The online version contains supplementary material available at https://doi.org/10.1007/s13201-021-01380-x.

Funding This work was supported by the Central Universities Fundamental Research Funds by Central South University (10400506021718).

Compliance with ethical standards

Conflict of interests The authors declare that they have no known competing financial interests or personal relationships that could have appeared to influence the work reported in this paper.

Informed consent Informed consent was obtained from all individual participants included in the study.

References

Aguila B, Sun Q, Cassady H, Abney CW, Li B, Ma S (2019) Design strategies to enhance amidoxime chelators for uranium recovery. ACS Appl Mater Interfaces 11:30919–30926. https://doi.org/10.1021/acsami.9b09532

Ahamed MI, Sharma G, Khan A, Asiri AM (2016) Turmeric/polyvinyl alcohol Th(IV) phosphate electrospun fibers: synthesis, characterization and antimicrobial studies. J Taiwan Inst Chem E 68:407–414. https://doi.org/10.1016/j.jtice.2016.08.024

Alakhras FA, Dari KA, Mubarak MS (2005) Synthesis and chelating properties of some poly(amidoxime-hydroxamic acid) resins toward some trivalent lanthanide metal ions. J Appl Polym Sci 97:691–696. https://doi.org/10.1002/app.21825

Al-Saleh MH, Sundararaj U (2011) Review of the mechanical properties of carbon nanofiber/polymer composites. *Composites*. Part A, Appl Sci Manuf 42:2126–2142. https://doi.org/10.1016/j.compositesa.2011.08.005

Anirudhan TS, Lekshmi GS, Shainy F (2019) Synthesis and characterization of amidoxime modified chitosan/bentonite composite for the adsorptive removal and recovery of uranium from seawater. J Coll Interf Sci 534:248–261. https://doi.org/10.1016/j.jcis.2018.09.009

Aslan T, Arslan S, Eyvaz M, Güçlü S, Yüksel E, Koyuncu İ (2016) A novel nanofiber microfiltration membrane: fabrication and characterization of tubular electrospun nanofiber (TuEN) membrane. J Membr Sci 520:616–629. https://doi.org/10.1016/j.memsci.2016.08.014

Bhardwaj N, Kundu SC (2010) Electrospinning: a fascinating fiber fabrication technique. Biotechnol Adv 28:325–347. https://doi.org/10.1016/j.biotechadv.2010.01.004

Blend-electrospun poly(vinylidene fluoride)/ polydopamine membranes: self-polymerization of dopamine and the excellent adsorption/separation abilities

Bui N, McCutcheon JR (2013) Hydrophilic nanofibers as new supports for thin film composite membranes for engineered osmosis. Environ Sci Technol 47:1761–1769. https://doi.org/10.1021/es304215g

Chandrashekhar Nayak M, Isloor AM, Inamuddin Lakshmi B, Marwani HM, Khan I (2020) Polyphenylsulfone/multiwalled carbon nanotubes mixed ultrafiltration membranes: fabrication, characterization and removal of heavy metals Pb2+, Hg2+, and Cd2+ from aqueous solutions. Arab J Chem 13:4661–4672. https://doi.org/10.1016/j.arabjc.2019.10.007

Chen Y, Jiang L (2020) Incorporation of UiO-66-NH2 into modified PAN nanofibers to enhance adsorption capacity and selectivity for oil removal. J Polym Res. https://doi.org/10.1007/s10965-020-2035-7

Chen W, Wang C, Gao Y, Wu Y, Wu G, Shi X, Du Y, Deng H (2020) Incorporating chitin derived glucosamine sulfate into nanofibers via coaxial electrospinning for cartilage regeneration. Carbohyd Polym 229:115544. https://doi.org/10.1016/j.carbpol.2019.115544

Ding Y, Wu J, Wang J, Lin H, Wang J, Liu G, Pei X, Liu F, Tang CY (2019) Superhydrophilic and mechanical robust PVDF nanofibrous membrane through facile interfacial Span 80 welding for excellent oil/water separation. Appl Surf Sci 485:179–187. https://doi.org/10.1016/j.apsusc.2019.04.214

Dognani G, Hadi P, Ma H, Cabrera FC, Job AE, Agostini DLS, Hsiao BS (2019) Effective chromium removal from water by polyaniline-coated electrospun adsorbent membrane. Chem Eng J 372:341–351. https://doi.org/10.1016/j.cej.2019.04.154

Dong H, Nyame V, MacDiarmid AG, Jones WE (2004) Polyaniline/poly(methyl methacrylate) coaxial fibers: The fabrication and effects of the solution properties on the morphology of electrospun core fibers. J Polym Sci, Part B: Polym Phys 42:3934–3942. https://doi.org/10.1002/polb.20253

Drosou C, Krokida M, Biliaderis CG (2018) Composite pullulan-whey protein nanofibers made by electrospinning: impact of process parameters on fiber morphology and physical properties. Food Hydrocoll 77:726–735. https://doi.org/10.1016/j.foodhyd.2017.11.014

Efome JE, Rana D, Matsuura T, Lan CQ (2018) Insight Studies on Metal-organic framework nanofibrous membrane adsorption and activation for heavy metal ions removal from aqueous solution. Acs Appl Mater Inter 10:18619–18629. https://doi.org/10.1021/acsami.8b01454

Fan J, Luo J, Zhang X, Zhen B, Dong C, Li Y, Shen J, Cheng Y, Chen H (2019) A novel electrospun β-CD/CS/PVA nanofiber membrane for simultaneous and rapid removal of organic micropollutants and heavy metal ions from water. Chem Eng J 378:122232. https://doi.org/10.1016/j.cej.2019.122232

Feng Z, Yuan X, Wang T (2020) Porous polyacrylonitrile/graphene oxide nanofibers designed for high efficient adsorption of chromium ions (VI) in aqueous solution. Chem Eng J 392:123730. https://doi.org/10.1016/j.cej.2019.123730

Fong H, Chun I, Reneker DH (1999) Beaded nanofibers formed during electrospinning. Polymer 40:4585–4592. https://doi.org/10.1016/S0032-3861(99)00068-3

Fu F, Wang Q (2011) Removal of heavy metal ions from wastewaters: a review. J Environ Manage 92:407–418. https://doi.org/10.1016/j.jenvman.2010.11.011

Habiba U, Afifi AM, Salleh A, Ang BC (2017) Chitosan/(polyvinyl alcohol)/zeolite electrospun composite nanofibrous membrane for adsorption of Cr6+, Fe3+ and Ni2+. J Hazard Mater 322:182–194. https://doi.org/10.1016/j.jhazmat.2016.06.028

Hong G, Li X, Shen L, Wang M, Wang C, Yu X, Wang X (2015) High recovery of lead ions from aminated polyacrylonitrile nanofibrous affinity membranes with micro/nano structure. J Hazard Mater 295:161–169. https://doi.org/10.1016/j.jhazmat.2015.04.020

Hou H, Ge JJ, Zeng J, Li Q, Reneker DH, Greiner A, Cheng SZD (2005) Electrospun polyacrylonitrile nanofibers containing a high concentration of well-aligned multiwall carbon nanotubes. Chem Mater 17:967–973. https://doi.org/10.1021/cm0484955

Hu L, Yan X, Yao C, Deng S, Gao X, Zhang X, Shan D (2016) Preparation of amidoximated coaxial electrospun nanofibers for uranyl uptake and their electrochemical properties. Sep Purif Technol 171:44–51. https://doi.org/10.1016/j.seppur.2016.07.024

Huang L, Manickam SS, McCutcheon JR (2013) Increasing strength of electrospun nanofiber membranes for water filtration using solvent vapor. J Membrane Sci 436:213–220. https://doi.org/10.1016/j.memsci.2012.12.037

Ishimura D, Morimoto Y (1998) Influences of chemical modifications on the mechanical strength of cellulose beads. Cellulose. https://doi.org/10.1023/A:1009277216057

Järup L (2003) Hazards of heavy metal contamination. Brit Med Bull 68:167–182. https://doi.org/10.1093/bmb/ldg032

Jobby R, Jha P, Yadav AK, Desai N (2018) Biosorption and biotransformation of hexavalent chromium [Cr(VI)]: a comprehensive review. Chemosphere 207:255–266. https://doi.org/10.1016/j.chemosphere.2018.05.050

Karki HP, Kafle L, Ojha DP, Song JH, Kim HJ (2019) Cellulose/polyacrylonitrile electrospun composite fiber for effective separation of the surfactant-free oil-in-water mixture under a versatile condition. Sep Purif Technol 210:913–919. https://doi.org/10.1016/j.seppur.2018.08.053

Kim H, Park SJ, Park CS, Le T, Hun Lee S, Ha TH, Kim H, Kim J, Lee C, Yoon H et al (2018) Surface-modified polymer nanofiber membrane for high-efficiency microdust capturing. *Chemical engineering journal (Lausanne*. Switzerland :1996 339:204–213. https://doi.org/10.1016/j.cej.2018.01.121

Kwak N, Jung WH, Park H, Hwang TS (2013) Electrospun polyethersulfone fibrous mats: sulfonation, its characterization and solution-phase ammonium sorption behavior. Chem Eng J 215–216:375–382. https://doi.org/10.1016/j.cej.2012.10.065

Lee KH, Kim HY, Bang HJ, Jung YH, Lee SG (2003) The change of bead morphology formed on electrospun polystyrene fibers. Polymer 44:4029–4034. https://doi.org/10.1016/S0032-3861(03)00345-8

Li L, Peng S, Lee JKY, Ji D, Srinivasan M, Ramakrishna S (2017) Electrospun hollow nanofibers for advanced secondary batteries. Nano Energy 39:111–139. https://doi.org/10.1016/j.nanoen.2017.06.050

Li J, Yang Y, Yu D, Du Q, Yang X (2018) Fast dissolving drug delivery membrane based on the ultra-thin shell of electrospun core-shell nanofibers. Eur J Pharm Sci 122:195–204. https://doi.org/10.1016/j.ejps.2018.07.002

Li T, Liu L, Zhang Z, Han Z (2020) Preparation of nanofibrous metal-organic framework filter for rapid adsorption and selective separation of cationic dye from aqueous solution. Sep Purif Technol 237:116360. https://doi.org/10.1016/j.seppur.2019.116360

Lu Y, He J, Luo G (2013) An improved synthesis of chitosan bead for Pb(II) adsorption. Chem Eng J 226:271–278. https://doi.org/10.1016/j.cej.2013.04.078

Mohammad A, Hussain S (2017) Inamuddin Sol–gel synthesis, physicochemical characterization, and analytical applications of copper selective composite cation exchanger: polyvinyl alcohol Ce(IV) phosphate. Polym Compos 38:332–340. https://doi.org/10.1002/pc.23591

Neghlani PK, Rafizadeh M, Taromi FA (2011) Preparation of aminated-polyacrylonitrile nanofiber membranes for the adsorption of metal ions: comparison with microfibers. J Hazard Mater 186:182–189. https://doi.org/10.1016/j.jhazmat.2010.10.121

Obaid M, Ghouri ZK, Fadali OA, Khalil KA, Almajid AA, Barakat NAM (2016) Amorphous SiO2 NP-Incorporated Poly(vinylidene fluoride) electrospun nanofiber membrane for high flux forward osmosis desalination. Acs Appl Mater Inter 8:4561–4574. https://doi.org/10.1021/acsami.5b09945

Ou K, Chen C, Lin L, Lu J, Shu Y, Tseng W, Yang J, Lee S, Chen C (2011) Membranes of epitaxial-like packed, super aligned electrospun micron hollow poly(l-lactic acid) (PLLA) fibers. Eur Polym J 47:882–892. https://doi.org/10.1016/j.eurpolymj.2011.02.001

Pereao O, Bode-Aluko C, Laatikainen K, Nechaev A, Petrik L (2019) Morphology, modification and characterisation of electrospun polymer nanofiber adsorbent material used in metal ion removal. J Polym Environ 27:1843–1860. https://doi.org/10.1007/s10924-019-01497-w

Puspitasari T, Kadja GTM, Radiman CL, Darwis D, Mukti RR (2018) Two-step preparation of amidoxime-functionalized natural zeolites hybrids for the removal of Pb2+ ions in aqueous environment. Mater Chem Phys 216:197–205. https://doi.org/10.1016/j.matchemphys.2018.05.083

Qu H, Wei S, Guo Z (2013) Coaxial electrospun nanostructures and their applications. J Mater Chem a 1:11513. https://doi.org/10.1039/c3ta12390a

Ren J, Yan C, Liu Q, Yang Q, Lu G, Song Y, Li Y (2018) Preparation of amidoxime-modified polyacrylonitrile nanofibrous adsorbents for the extraction of copper(II) and lead(II) ions and dye from aqueous media. J Appl Polym Sci 135:45697. https://doi.org/10.1002/app.45697

Saeed K, Haider S, Oh T, Park S (2008) Preparation of amidoxime-modified polyacrylonitrile (PAN-oxime) nanofibers and their applications to metal ions adsorption. J Membrane Sci 322:400–405. https://doi.org/10.1016/j.memsci.2008.05.062

Sagitha P, Reshmi CR, Sundaran SP, Sujith A (2018) Recent advances in post-modification strategies of polymeric electrospun membranes. Eur Polym J 105:227–249. https://doi.org/10.1016/j.eurpolymj.2018.05.033

Sethurajan M, van Hullebusch ED, Nancharaiah YV (2018) Biotechnology in the management and resource recovery from metal bearing solid wastes: recent advances. J Environ Manage 211:138–153. https://doi.org/10.1016/j.jenvman.2018.01.035

Seyyed Monfared Zanjani J, Saner Okan B, Letofsky-Papst I, Yildiz M, Menceloglu YZ (2015) Rational design and direct fabrication of multi-walled hollow electrospun fibers with controllable structure and surface properties. Eur Polym J 62:66–76. https://doi.org/10.1016/j.eurpolymj.2014.10.019

Sun Q, Yang Z, Hu C, Li C, Yan G, Wang Z (2020) Facile preparation of superhydrophobic PVDF microporous membranes with excellent anti-fouling ability for vacuum membrane distillation. J Membr Sci 605:118106. https://doi.org/10.1016/j.memsci.2020.118106

Thavasi V, Singh G, Ramakrishna S (2008) Electrospun nanofibers in energy and environmental applications. Energ Environ Sci 1:205. https://doi.org/10.1039/b809074m

Wang H, Zhou A, Peng F, Yu H, Yang J (2007) Mechanism study on adsorption of acidified multiwalled carbon nanotubes to Pb(II). J Colloid Interf Sci 316:277–283. https://doi.org/10.1016/j.jcis.2007.07.075

Wang B, Xia J, Mei L, Wang L, Zhang Q (2017) Highly efficient and rapid lead(II) scavenging by the natural artemia cyst shell with unique three-dimensional porous structure and strong sorption affinity. Acs Sustain Chem Eng 6:1343–1351. https://doi.org/10.1021/acssuschemeng.7b03667

Wang M, Li X, Zhang T, Deng L, Li P, Wang X, Hsiao BS (2018) Eco-friendly poly(acrylic acid)-sodium alginate nanofibrous hydrogel:

a multifunctional platform for superior removal of Cu(II) and sustainable catalytic applications. Coll Surf, A 558:228–241. https://doi.org/10.1016/j.colsurfa.2018.08.074

Wang D, Yue Y, Wang Q, Cheng W, Han G (2020) Preparation of cellulose acetate-polyacrylonitrile composite nanofibers by multi-fluid mixing electrospinning method: Morphology, wettability, and mechanical properties. Appl Surf Sci 510:145462. https://doi.org/10.1016/j.apsusc.2020.145462

Wu CM, Chou MH (2016) Polymorphism, piezoelectricity and sound absorption of electrospun PVDF membranes with and without carbon nanotubes. Compos Sci Technol 127:127–133. https://doi.org/10.1016/j.compscitech.2016.03.001

Wu Y, Pang H, Liu Y, Wang X, Yu S, Fu D, Chen J, Wang X (2019) Environmental remediation of heavy metal ions by novel-nanomaterials: a review. Environ Pollut 246:608–620. https://doi.org/10.1016/j.envpol.2018.12.076

Xiao J, Jing Y, Yao Y, Wang X, Jia Y (2019) Synthesis of amidoxime-decorated 3D cubic mesoporous silica via self-assembly co-condensation as a superior uranium(VI) adsorbent. J Mol Liq 277:843–855. https://doi.org/10.1016/j.molliq.2019.01.009

Xiaolei Qu, Pedro JJ (2013) Applications of nanotechnology in water and wastewater treatment. Water Res. https://doi.org/10.1016/j.watres.2012.09.058

Yin W, Li M, Hu T, Xue Z, Yu J, Chi R (2018) Preparation of an adsorbent based on amidoxime and triazole modified waste cotton fabrics through an Azide-Alkyne click reaction with excellent adsorption performance toward Cu(II). Acs Sustain Chem Eng 7:1944–1955. https://doi.org/10.1021/acssuschemeng.8b04104

Yuan Q, Fu Z, Wang Y, Chen W, Wu X, Gong X, Zhen D, Jian X, He G (2020) Coaxial electrospun sulfonated poly (ether ether ketone) proton exchange membrane for conductivity-strength balance. J Membr Sci 595:117516. https://doi.org/10.1016/j.memsci.2019.117516

Zhang C, Yuan X, Wu L, Han Y, Sheng J (2005) Study on morphology of electrospun poly(vinyl alcohol) mats. Eur Polym J 41:423–432. https://doi.org/10.1016/j.eurpolymj.2004.10.027

Zhang S, Shi Q, Christodoulatos C, Meng X (2019) Lead and cadmium adsorption by electrospun PVA/PAA nanofibers: batch, spectroscopic, and modeling study. Chemosphere 233:405–413. https://doi.org/10.1016/j.chemosphere.2019.05.190

Zhao D, Sheng G, Hu J, Chen C, Wang X (2011) The adsorption of Pb(II) on Mg2Al layered double hydroxide. Chem Eng J 171:167–174. https://doi.org/10.1016/j.cej.2011.03.082

Zheng L, Zhang S, Cheng W, Zhang L, Meng P, Zhang T, Yu H, Peng D (2019) Theoretical calculations, molecular dynamics simulations and experimental investigation of the adsorption of cadmium(ii) on amidoxime-chelating cellulose. J Mater Chem a 7:13714–13726. https://doi.org/10.1039/c9ta03622a

Zhijiang C, Xianyou S, Qing Z, Yuanpei L (2017) Amidoxime surface modification of polyindole nanofiber membrane for effective removal of Cr(VI) from aqueous solution. J Mater Sci 52:5417–5434. https://doi.org/10.1007/s10853-017-0786-2

Zhu F, Lu Y, Li L (2016) Synthesis, adsorption kinetics and thermodynamics of ureido-functionalized Pb(ii) surface imprinted polymers for selective removal of Pb(ii) in wastewater. Rsc Adv 6:11112–111128. https://doi.org/10.1039/c6ra18736f

Zhuang S, Cheng R, Kang M, Wang J (2018) Kinetic and equilibrium of U(VI) adsorption onto magnetic amidoxime-functionalized chitosan beads. J Clean Prod 188:655–661. https://doi.org/10.1016/j.jclepro.2018.04.047